| Journal of Coastal Research | 28 | 6 | 1426–1436 | Coconut Creek, Florida | November 2012 |
|---|---|---|---|---|---|

# Integration of Optical and Acoustic Remote Sensing Data over the Backshore–Foreshore–Nearshore Continuum: A Case Study in Ostend (Belgium)

**Luc Bertels[†*], Rik Houthuys[†], Bart Deronde[†], Rindert Janssens[‡], Els Verfaillie[§], and Vera Van Lancker[††]**

[†]Flemish Institute for Technological Research
Department of Remote Sensing and Earth Observation Processes
Boeretang 200
B-2400 Mol, Antwerp, Belgium
luc.bertels@vito.be

[‡]Ghent University
Geology and Soil Science
Renard Center of Marine Geology
Krijgslaan 281, S-8,
B-9000, Gent, Belgium

[§]Ghent University
Geography
Carto-GIS Cluster
Krijgslaan 281, S-8
B-9000, Gent, Belgium

[††]Royal Belgian Institute of Natural Sciences
Management Unit of the North Sea Mathematical Models
Gulledelle 100
B-1200, Brussels, Belgium

www.cerf-jcr.org

www.JCRonline.org

**ABSTRACT**

Bertels, L.; Houthuys, R.; Deronde, B.; Janssens, R.; Verfaillie, E., and Van Lancker, V., 2012. Integration of optical and acoustic remote sensing data over the backshore–foreshore–nearshore continuum: a case study in Ostend (Belgium). *Journal of Coastal Research,* 28(6), 1426–1436. Coconut Creek (Florida), ISSN 0749-0208.

This research addresses the possibilities of the combined use of airborne hyperspectral imaging spectroscopy, airborne laser scanning, and seaborne sonar to study the sediment dynamics in the back-, fore-, and nearshore continuum. In May 2009, airborne light detection and ranging (LiDAR) and hyperspectral data were acquired at low tide of the beach in Ostend, Belgium. In June 2009, seaborne side-scan sonar and single- and multibeam depth and backscatter data were acquired in the nearshore part of the Ostend coastal area at high tide. Both LiDAR and single- and multibeam data were used to create a topographic reference of the back- to nearshore continuum, with an average vertical accuracy of 10 cm. This reference framework was used, in combination with historical data, to study the morphological evolution over the last few years. Hyperspectral data, optionally combined with LiDAR-derived intensity, slope, and elevation data, were used for sedimentological mapping of the back- and foreshore area. Both multibeam backscatter and side-scan sonar data were used to produce a sedimentary surface facies map of the nearshore area. Because no automatic classification of subtle seabed gradients is yet available, the data were manually screened to produce 12 sedimentary classes. Subsequently, the airborne- and seaborne-derived maps were combined to construct an integrated sedimentological and morphological map of the entire area. This was used to interpret and formulate statements about the sediment dynamics of the area.

**ADDITIONAL INDEX WORDS:** *Imaging spectroscopy, light detection and ranging (LiDAR), side-scan sonar, single-beam echo sounder, multibeam echo sounder, sedimentological map, morphological map, linear discriminant analysis, monitoring, beach nourishment.*

## INTRODUCTION

The Belgian coastline is a sandy beach barrier that stretches for 65 km from De Panne, on the French border, to Knokke, near the Dutch border. The geomorphology of the Belgian coast comprises a gently sloping and fine-sand beach; a dune ridge generally less than 20 m high, varying in width from a few kilometers (De Panne, east of Knokke) to less than 100 m; and a backing coastal plain up to 15 km wide (De Moor, 2006). At present, more than 50% of the coast suffers erosion (Deronde *et al.,* 2006). Wind-driven waves and storms play an important role in the short-term coastal evolution (*e.g.,* Smith *et al.,* 2000; Stone and Orford, 2004). During high-energy events, significant beach erosion can occur within a few hours, while beach and dune recovery to reestablish the former morphology may take many years (*e.g.,* Maspataud, Ruz, and Héquette, 2009). A rise in sea level as a result of global warming is another threat (Leatherman, Zhang, and Douglas, 2000).

Often, the morphosedimentary state and dynamics of coastal processes determine how well beach sections recover from erosive events or whether sufficient sediment is available to cope with a rise in sea level. For this reason, a realistic estimation of the coastal sediment budget is crucial and requires data from the coastal dunes down to the seabed. Studies are mostly limited to the beach and only occasionally include the nearshore; when they do, the nearshore is often studied as a separate entity. However, coastal processes act over the continuum of the dunes and back-, fore-, and nearshore (hereafter called the inshore) and even offshore (*e.g.,* Dean and Dalrymple, 2004). Morphological and sedimentological processes caused by human interventions have been monitored, but mostly without considering the inshore contin-

*DOI:10.2112/JCOASTRES-D-12-00004.1 received 5 January 2012; accepted in revision March 23, 2012.*
Published Pre-print online 25 June 2012.

uum (*e.g.,* Deronde *et al.,* 2006, 2008a, 2008b). Consequently, there are major gaps in our knowledge on the sediment dynamics. Meanwhile, marine nature reserves are being planned in the near- to offshore zone that need adequate management and monitoring tools. In this context, the morphosedimentary state and dynamics are important, because they can also provide an indirect estimate of biodiversity (Van Lancker *et al.,* 2012).

However, investigating the inshore continuum requires combining different techniques and approaches and subsequently different know-how and skills. The dune, backshore, and foreshore can be monitored using airborne techniques, while in turbid coastal areas such as in the North Sea, acoustic techniques are needed for the near- to offshore. As such, different scientific disciplines are involved, and this has implications for the analysis of the techniques used. Moreover, the morphosedimentological hypotheses that arise from the results only apply to one section of the most dynamic part of the coastal zone. To produce spatially integrated maps of the morphosedimentary environment, know-how and expertise from both the airborne and the seaborne realms need to be combined.

## STUDY AREA

For this study, a dynamic coastal site presenting various interests and challenges in a small area was selected: the beach at Ostend city center (Figure 1). Here, the seafront wall juts out up to 200 m from to the surrounding coastline. The historic town of Ostend was originally located here and was held in place by coastal defenses from the 16th to the 20th century, while the surrounding coast was allowed to erode and thus retreat. In the beginning of the 2000s, the coastal safety of Ostend center, where severe floods occurred in 1953, was evaluated by the Flemish coastal authorities to be the lowest at the Belgian coast with acute risk of overtopping and breaching of the existing old seawall (*e.g.,* Mertens *et al.,* 2008; 2011). For public safety, "emergency" beach nourishment was carried out in 2004. This emergency fill was meant to raise the safety level immediately while awaiting the construction of the new western harbor dam in 2010–11, which will probably give rise to a naturally accreting coast. To allow the study of possible transfer of nourishment sand across the harbor channel, a small strip of the coast east of Ostend was included in the study area.

The study area was defined to include section 109, just east of Mariakerke, where yearly small-scale beach fills maintain a dry backshore berm in front of the seawall. The eastern sections 119 to 123 have a hard seawall on top of which sits a dune ridge. The eastern part is more "natural" in the sense that no nourishment events have been conducted there. The length of the study area is 4250 m, with a mean width from the seawall outward of 1200 m. All elevations used are in the Belgian standard datum of tweede algemene waterpassing (TAW), whose 0 m corresponds approximately to the local mean low low water springs (MLLWS) level. The tidal range at Ostend is 3.5 m at neap tide and 5.0 m at spring tide. The mean width of the intertidal beach is approximately 150 m. A small

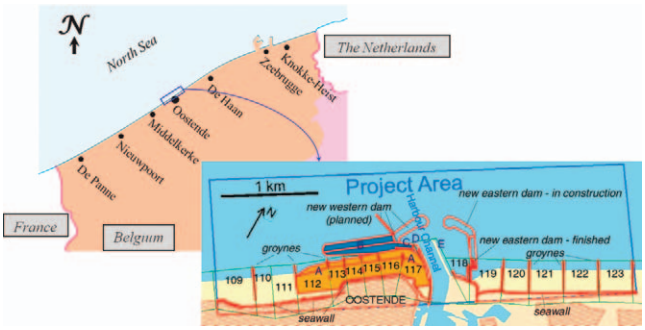


Figure 1. Study area location along the Belgian coast. The detail shows site features and coastal section numbers. Beach sections are outlined and represent the standard spatial units used in routine morphological monitoring at the Belgian shore. West of section 109 is the sea resort of Mariakerke. Sections 109 to 113 are Large Beach (Groot Strand). Sections 113 to 116 correspond to the formerly narrow beach in Ostend center. Section 117 is Little Beach (Klein Strand). In section 118, the beach has practically disappeared and is included in the harbor mouth area. The marked areas are (A) area of emergency beach nourishment (the seaward part is the slope connecting the raised beach to the existing shoreface), (B) area of underwater nourishment (the lower half is a flat-top area, and the upper half is the connecting slope), (C) area of underwater grit fill, (D) old west pier (a protected construction to be maintained), and (E) old east pier (demolished at the time of the study). The old access to Ostend harbor is marked by the text "Harbor Channel." The new access channel is a few hundred meters to the east, but apart from some preparatory dredging, the old channel was still in use during the study. (Color for this figure is only available in the online version of this paper.)

strip hugging the seawall is situated at +6 m TAW and is only flooded at high tide during extreme storms.

Before 2004, Ostend center beach consisted of a narrow strip at low tide and no beach at high tide. In 2004, so-called emergency nourishment was carried out aimed at increasing the safety level so that it would withstand a 1000-year return period storm (allowed overtopping of 1 L/m/s). Nourishment raised the beach profile to create, at high tide, a strip of dry beach about 200 m wide. In the initial nourishment design, the fill started at elevation +4 m TAW downward (red line in Figure 2). While the works were in progress, the decision was made to create an evacuation strip for beach visitors situated at +6 m TAW (green line in Figure 2). The fills involved the supply of 700,000 $m^3$ of sand (red and green profiles) and another 100,000 $m^3$ of sand for the underwater part (blue line in Figure 2).

The median grain size before nourishment was approximately 200 μm. The median grain size after nourishment was 300 to 350 μm, locally up to 400 μm. The sand was borrowed from offshore sites and from in and around major shipping lanes. Emergency nourishment started in April 2004 and ended in June 2004. Afterward, erosion was observed in the high-water swash zone, which, within a period of several months, drastically reduced the fill above +2 m TAW (De Wolf *et al.,* 2006). The lower part of the intertidal zone and the strip between the underwater ridge and the intertidal beach, situated between –0.5 and –2 m TAW, accreted. In section 117, a high-water spit developed that gradually extended

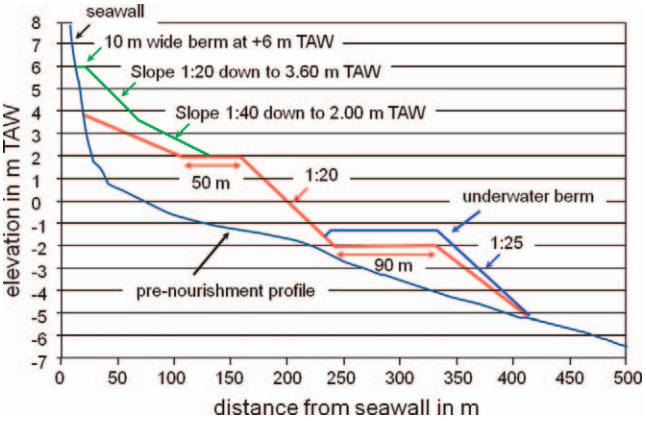


Figure 2. Beach profile before and after nourishment work (International Marine & Dredging Consultants). (Color for this figure is only available in the online version of this paper.)

eastward and finally touched the harbor channel. Redistribution of grain size areas was observed, with a major increase around +3 m TAW, due to local deposition of shell fragments. After 2004, several refills had to be carried out to restore subsequent erosional stages. To summarize, more than 1 million $m^3$ of sand has been added to the beach at Ostend center. Of this, more than 350,000 $m^3$ was filled in successive years following the large-scale 2004 emergency nourishment. In 2009, beach scraping was performed in late spring, but before the inshore surveys.

## METHODOLOGY

### Overview of the Data Collection Campaigns

Both historical and newly acquired data sets (Table 1) were used. The Coastal Division of the Flemish Authorities collects echo-sounding data annually for bathymetric mapping of the nearshore and parts of the offshore area along the entire Belgian coast. Light detection and ranging (LiDAR) data are also collected yearly and were used for topographic mapping and volumetric budget calculations. Specifically for this study, hyperspectral, LiDAR, and side-scan sonar campaigns (Figure 3) were conducted, in combination with collection of the necessary ground reference data. Low-density (1 pulse/$m^2$) LiDAR data, collected on 24 May 2009, were provided by the Coastal Division.

The airborne hyperspectral campaign used the Itres Compact Airborne Spectrographic Imager (CASI) 1500. This system was used to acquire image data in 18 spectral bands (Figure 4).

Data acquisition took place according to the following specifications: "Data acquisition should take place as soon as possible, preferably in May 2009 and not later than the end of July 2009. Use is to be made of the tidal sea level oscillation to create an overlap between subaerial and subaquatic surveys. The hyperspectral data acquisition should take place between one hour before and one hour after low tide and between three hours before and three hours after the highest position of the sun. The sonar recordings on the beach should be carried out during high tide."

Table 1. *Overview of historical and newly acquired data sets.*

| Date | Survey | Remark |
|---|---|---|
| 1–15/04/2004 | Echo sounding | Just before the start of nourishment work |
| 17/04/2004 | LiDAR | Just before emergency nourishment work |
| 1–15/06/2004 | Echo sounding | Just after nourishment work ended |
| 23/08/2005 | LiDAR | |
| 18/04/2006 | LiDAR | |
| 3/06/2007 | LiDAR | |
| 19/06/2008 | LiDAR | |
| 13/05/2009 | Field survey | Preaerial field inspection |
| 24/05/2009 | LiDAR | |
| 29/05/2009 | Hyperspectral imaging | Inshore airborne survey using the CASI 1500 |
| 29/05/2009 | Field survey | Inshore during survey fieldwork on the beach |
| 12/06/2009 | Echo sounding | |
| 23–26/06/2009 | Echo sounding | Inshore side-scan sonar data acquisition |
| 22, 24, 30/06/2009 | Field survey | Inshore subaquatic sediment sample collection |
| 30/06–2/07/2009 | Echo sounding | Inshore multibeam sonar data acquisition |

The hyperspectral data were acquired on 29 May 2009 and were received, radiometrically corrected, by the Flemish Institute for Technological Research (VITO) by the end of July 2009. These data were subsequently preprocessed for atmospheric and geometric correction in the Central Data Processing Center at VITO and resampled to $1 \times 1$ m pixels.

The side-scan sonar campaigns took place on 23 and 26 June 2009 using the Klein 3000 towed by the *Last Freedom,* a small vessel that made it possible to sail close to the shoreline (Table

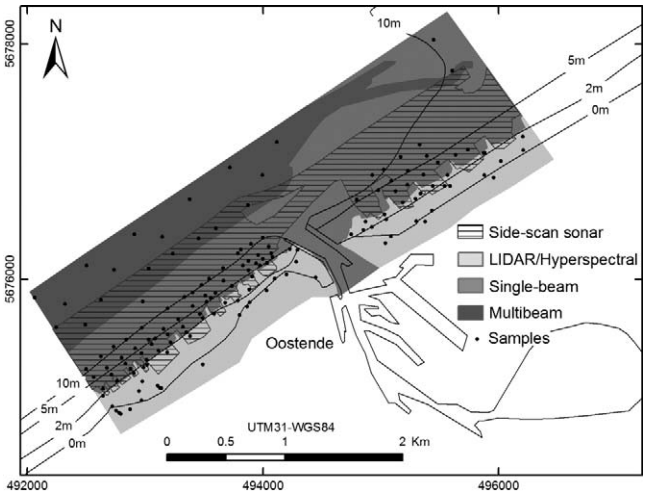


Figure 3. Map of the inshore area showing the locations where the different data sets were collected.

| CASI 1500 Specifications | |
|---|---|
| Field of View | 40° across-track over 1500 pixels |
| Spectral range | 650 nm between 380 and 1050 nm |
| Spectral samples | programmable, up to 288 (< 3.5 nm FWHM) |
| Aperture | F/3.5 to F/18.0 |
| Dynamic range | 16,384:1 (14 bits) |
| Noise floor | 3.0 DN |
| Signal to noise ratio | 800:1 peak |
| Sustained data range | 9 Megapixel/sec |

| Channel nr. | Central Wavelength (nm) | FWHM (nm) |
|---|---|---|
| 1 | 107.2 | 12.9 |
| 2 | 443.4 | 14.5 |
| 3 | 488.4 | 9.7 |
| 4 | 508.7 | 8.0 |
| 5 | 530.0 | 10.5 |
| 6 | 550.3 | 6.6 |
| 7 | 569.4 | 9.0 |
| 8 | 633.4 | 7.1 |
| 9 | 652.8 | 2.5 |
| 10 | 664.4 | 1.3 |
| 11 | 672.4 | 1.3 |
| 12 | 689.0 | 1.4 |
| 13 | 703.5 | 1.5 |
| 14 | 709.5 | 1.5 |
| 15 | 747.5 | 1.7 |
| 16 | 778.5 | 1.8 |
| 17 | 815.9 | 1.9 |
| 18 | 867.0 | 12.8 |

Figure 4. CASI 1500 sensor characteristics and band settings used for this study.

2). The sonar uses two frequencies, 100 and 500 kHz. Data processing, including mosaicking at 1 × 1 m, was done using SonarScope (Ifremer). Both frequencies were used to interpret the sedimentological characteristics of the intertidal and offshore seafloor. The lower frequency penetrates through the upper mud layers, while the higher frequency detects the top layers.

Both multibeam bathymetry and multibeam backscatter data were recorded during the *RV Belgica* campaign ST0917 from 30 June to 2 July 2009. Data were collected using a Simrad EM3002 dual-head system with a working frequency of 300 kHz (Table 3). The system has roll stabilized beams and is therefore accurate in shallow water. Although the western part of the study area was well covered, the eastern part was not. Ongoing offshore construction works and diving activity at the time of data acquisition made navigation in this part of the study area impossible. *RV Belgica* could not access the shallowest part of the nearshore area, which was covered by side-scan sonar. Multibeam data were also processed in SonarScope and gridded to 1 × 1 m pixels.

The fieldwork for documenting the sand classes of the beach was conducted simultaneously with the hyperspectral flight on 29 May 2009. A total of 59 samples were taken at areas representing the classes identified in a preaerial field survey on 13 May 2009. Care was taken to collect samples in homogeneous-looking areas. Each time, the Differential Global Positioning System (dGPS) position was recorded and at least two photos were taken, one showing the sample location in its surrounding context and the other showing a close-up of the beach surface at the sample location. About 0.5 kg of sand was scraped off the top 0.5-cm layer. The seabed was sampled using a Van Veen grab that removes sediment from the top 5 to 10 cm of the seabed. A total of 96 subaquatic sediment samples were taken during the side-scan sonar and multibeam campaigns on 24 and 30 June 2009. The northern area was less densely sampled due to the presence of numerous buoys, which made navigation difficult. The samples were analyzed for grain size distribution (*e.g.*, median grain size and mud content), organic material, and calcium carbonate content.

## Classification of the Hyperspectral Image

Geographic information concerning the 59 subaerial field locations was used to extract reference spectra from the georeferenced hyperspectral images. A class number and name were assigned to each location according to the observations made in the field. The different targeted classes were easily recognized in the field (Figure 5).

In the first classification trial, the pixel spectra of a rectangle of 3 × 3 pixels (called a region of interest, or ROI), centered on the labeled sample location, were stored in a reference spectral library and given the corresponding class label. For classes with a locally restricted occurrence, such as shell patches, care was taken to sample the spectra of pixels belonging to the patch. Because the classification revealed some differences from the sand structure classes observed in the field, the ROIs were enlarged to increase the number of

Table 2. *The Klein 3000 digital side-scan sonar system on board the* Last Freedom, *used to collect side-scan sonar data*. (Color for this table is only available in the online version of this paper.)

| | |
|---|---|
| Frequencies (kHz) | 100 (125 ± 1% act.)<br>500 (445 ± 1% act.) |
| Transmission pulse | Tone burst, operator selectable, 25–400 users<br>Independent pulses for each frequency |
| Beams | |
| Horizontal | 1° at 100 kHz, 0.2° at 500 kHz |
| Vertical | 40° |
| Beam tilt | 5°, 10°, 15°, 20°, and 25° down, adjustable |
| Maximum range (m) | 600 at 100 kHz, 150 at 500 kHz |
| Depth rating | 1500 m standard, options to 3- and 6-km depths |
| Construction | Stainless steel |
| Size (cm) | 122 length, 8.9 diameter |
| Weight (kg in air) | 28 |

Table 3. *The EM3002 dual-head multibeam system on board the* RV Belgica. (Color for this table is only available in the online version of this paper.)


| | |
|---|---|
| Frequencies (kHz) | 293, 300, 307 |
| Number of soundings *per* ping: | |
| Maximum single sonar head | 254 |
| Maximum dual sonar heads | 508 |
| Maximum ping rate (Hz) | 40 |
| Maximum angular coverage | |
| Single sonar head | 130° |
| Dual sonar heads | 200° |
| Pitch stabilization | Yes |
| Roll stabilization | Yes |
| Heave compensation | Yes |
| Pulse length (μs) | 150 |
| Range sampling rate (kHz) | 14, 14.3, 14.6 |
| Depth resolution (cm) | 1 |

reference spectra (Table 4). This could be achieved in a Geographic Information System (GIS) environment by using a visual presentation of the hyperspectral image and the classified image, in combination with visualizing and interpreting the field pictures. Two additional classes were defined to cover the small areas of water and algae present in the image. The reference spectra extracted from the ROIs were used to train a linear discriminant analysis classifier (Kempeneers *et al.,* 2004). Also, a regrouping scheme of the 16 detailed classes into 8 workable classes was worked out to allow comparison with older hyperspectral classifications of the area. Merging was based on the physical and chemical properties of the sediment samples, combined with their appearance on the beach (Table 4).

## Classification of the Acoustic Data

Automated acoustic image classification is yet not advanced enough to detect subtle gradients within a mud to sandy sediment gradient. A manual procedure was thus used, and acoustic facies were delineated in GIS. Imagery from both side-scan sonar and multibeam data were loaded one by one in the GIS, where they were scrutinized interactively, based on differences in their texture and intensity. Both frequencies of side-scan sonar were used in the interpretation, though most information was derived from the 100-kHz transducer. The working scale was 1:250, which rendered the finest details in the image visible while showing a sufficiently large part of the image to still have an overview of the area. Overlapping images were used in areas where interpretation was difficult. The first processing step resulted in preliminary bed structure classes with sufficient distinguishing characteristics. Figure 6 shows the delineation of class A5, homogeneous flat areas, as an example. Classes showing sharp-crested, subaqueous dunes demonstrate mobile beds. The mobile dunes occur around the harbor dam extension under construction. A few weeks before the inshore surveys, dredged sand was dumped at the shoreface site of the new eastern harbor dam. Bathymetric monitoring showed that this sand had been redistributed by the currents. The area of occurrence of the dune class clearly demonstrates the extent of this process of sand redistribution.

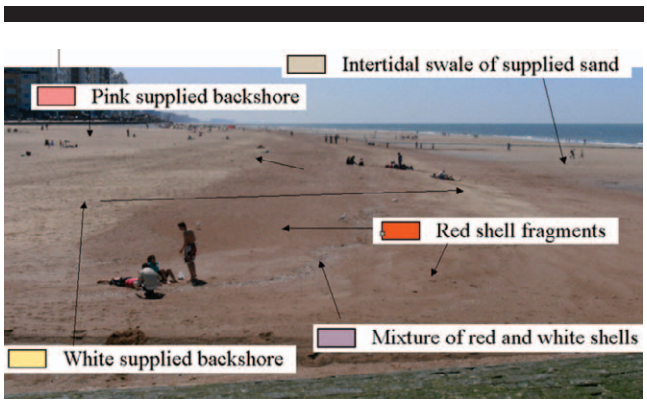


Figure 5. Scene of the western part of Ostend beach clearly showing the transition from the backshore classes to the intertidal classes. (Color for this figure is only available in the online version of this paper.)

In successive passages, the images were geographically partitioned into the different classes. Although most of the classes were well delineated, some showed a gradual transition. Even for the well-delineated classes, the boundaries outlining the classes should in most cases be considered not sharp boundaries but rather gradual transitions in a relatively narrow strip.

The acoustic classes present offshore prove that the seabed is swept by currents. A clear illustration of this natural process is the eastern harbor dam construction area where, in a matter of weeks, dumped sand has been lowered by more than 0.5 m and is actively being spread by dune motion over several hectares downstream (with respect to the dominant flood current). From morphological monitoring, this area proves to be erosive. The active dunes are thus the conveyor belt of sand leaving the area. The dredged harbor access channel is a likely local sink, because it has to be kept at a depth 1 to 2 m below the surrounding seabed by dredging. Morphological monitoring shows ongoing sedimentation between dredging works. The acoustic class found in the harbor access channel is representative of mud covered with (thin) sand patches. It is interpreted as fresh sedimentation.

Table 4. *Ground reference data for 16 classes, based on ground locations from the field campaign and manually extended.*

| Class | Class Name | ROIs | Pixels | Merged Class |
|---|---|---|---|---|
| H1 | Aeolian sand | 2 | 343 | D9 |
| H2 | Backshore berm sand | 3 | 769 | D5 |
| H3 | Mixed backshore slope sand–flood mark–white shells | 2 | 21 | D5 |
| H4 | Backshore slope sand | 5 | 1484 | D4 |
| H5 | Shallow intertidal sand | 2 | 652 | D4 |
| H6 | Intertidal shoals sand | 7 | 2547 | D3 |
| H7 | Intertidal swales sand | 6 | 2041 | D3 |
| H8 | Dark intertidal flat sand | 5 | 1418 | D2 |
| H9 | Yellow supplied backshore sand | 2 | 381 | D7 |
| H10 | Pink supplied backshore sand | 3 | 712 | D7 |
| H11 | White supplied backshore slope sand | 2 | 157 | D5 |
| H12 | Intertidal shoal of supplied sand | 7 | 2547 | D7 |
| H13 | Intertidal swale of supplied sand | 6 | 2041 | D7 |
| H14 | Red shell fragments | 3 | 518 | D8 |
| H15 | Wet red shell fragments | 1 | 175 | D8 |
| H16 | Mixture of red and white shell fragments | 3 | 471 | D8 |

## RESULTS AND DISCUSSION

### The Integrated Sedimentary Surface Facies Map

Figure 7 shows the classification result of the Ostend beach area obtained from the hyperspectral image. The first eight classes are intended to represent the "natural" Belgian beach profile. These classes were defined on the beach, east of the harbor channel. The second eight classes are intended to represent the nourishment area in Ostend center, west of the harbor channel, where characteristic, reddish sediment was supplied. To judge the performance of the classification, the classification result was validated using a confusion matrix. This validation method directly compares the classification result with the ground reference data defined *via* the ROIs. The average accuracy was 96% with a kappa of 0.96. The reason for the extremely high classification accuracy is good field

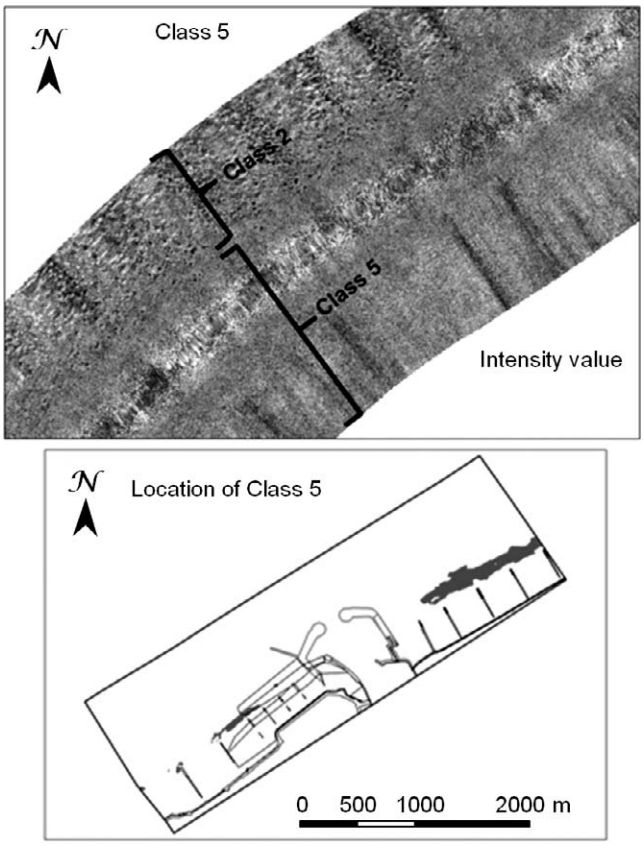


Figure 6. (top) Example of a side-scan sonar image typifying class A2, macrobenthos patches, and class A5, homogeneous flat areas. (bottom) The occurrence of class A5 in the study area.

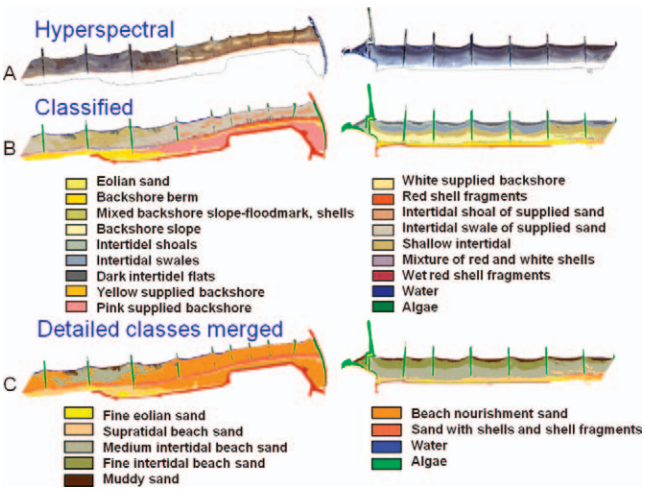


Figure 7. (A) Cutout from the hyperspectral image. (B) Detailed classification with 18 classes. To get a workable map, the former 16 detailed classes are merged to 8 classes. The area shown is approximately 4 km long. (Color for this figure is only available in the online version of this paper.)

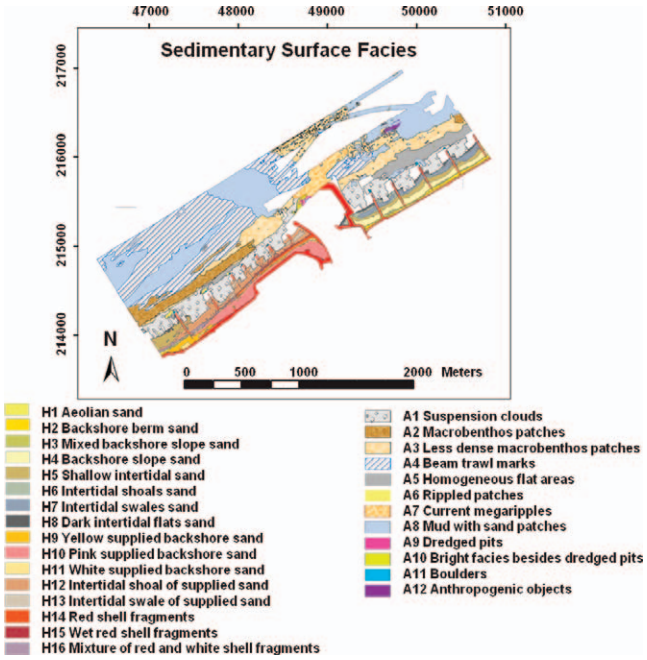


Figure 8. Final classification of the inshore area, *i.e.,* the integrated sedimentary surface facies map, combining the manually obtained, the subtidal sediment classes and the automatically obtained airborne classification of the beach. (Color for this figure is only available in the online version of this paper.)

knowledge when defining the ground reference data and the ROIs. The ROIs were defined on large homogeneous areas and carefully identified in the field; thus, they represent pure end members. They contained numerous reference spectra, which captured the subtle spectral variation within each class. All of this helped to optimize the spectral separability of the 16 classes.

To obtain a workable map and for comparison with hyperspectral data from previous projects, the detailed classes were merged into the eight classes used earlier. This was done by grouping classes into new ones in a predefined way, as shown in Table 4. Validation of the merged classification led to an average accuracy of 98% and a kappa of 0.97.

Additional attempts were undertaken using the LiDAR intensity, elevation, and slope data as supplementary layers of information to the hyperspectral data. Although useful information is contained in these extra bands, the information was already available in the hyperspectral recordings. Therefore, the extra bands did not improve the classification and were discarded.

Figure 8 shows the integrated sediment surface facies map, containing the sixteen supratidal and twelve subtidal sediment classes. Although the intention was to create sufficient overlap between airborne and acoustic data, an overlap of only 60 m was achieved. In this overlap area, the airborne and the acoustic data sets failed to produce classes representing identical ground features. The reason for this failure was differing dynamic conditions. During the airborne survey, the beach was maximally exposed, and no sediment transport was going on in the lowermost part of the beach. During the sonar recordings at high tide, waves and the maneuvering of the survey vessel in the shallowest parts stirred the bed sediment. The effect was that the two data sets—the seaborne sonar recordings and the airborne hyperspectral recordings—were acquired in two completely different mediums and consequently map different objects. Unfortunately, due to the presence of many "suspension clouds," acoustic surveys of the extremely shallow intertidal beach at high tide proved impossible. The only object type that was clearly recognizable in both data sets was the groins. The deeper zones of the subtidal part show bed structures that are typical of either wave or current action, grading into classes and indicating more stable beds. The supratidal area is dominated by the beach, which is wave built: from relatively fine sand near the low-water mark to coarser sand at the high-water mark. The wave action wipes out any bedform that could be captured by remote sensing. On the other hand, hyperspectral remote sensing is sensitive to spectral signatures and therefore well suited to detect different sand types, which is why the sand used for the beach nourishment sand was easily recognized.

## Sedimentological Interpretation

Figure 9 shows the results of analysis of the sediment samples overlaid on the integrated sedimentary surface facies map. On the beach and the shoreface, the median grain size was coarser in the western part of the study area than in the eastern part. This is the direct result of the nourishment events in the western zone in the recent past. The nourished sand had a larger median grain size (350 to 500 μm) than the grain size (150 to 250 μm) in the eastern part of the natural beach. In the eastern part, the grain size gradient from the high-water mark (250 μm) to the low-water mark (180 μm) and farther down to the shoreface (125–150 μm) corresponds to the grain size gradient of the sand on the natural beach. Slightly coarser samples on the shoreface correspond to submerged bar crests. The flat seabed generally consists of fine sand, although slightly coarser samples were also found. These were probably sediment lags (coarser sand that is not in active transport during fair weather), because they are isolated samples surrounded by much finer sand. In the nourishment zone, the median grain size was large, around 350 to 400 μm, corresponding to the coarser sand supplied there. Contrary to what we might expect, the shoreface was fine grained, even in the vicinity of the nourishment zone. At this distance from the low-water mark, there was no contrast with the "natural" eastern part.

Concerning $CaCO_3$ content, there is an overall increase from the beach to the offshore area. $CaCO_3$ is due to the presence of shell debris, where the high concentrations on the flat seabed may be another indication of to sediment lags. On the beach, near the groins, the high concentration of $CaCO_3$ is due to the local accumulation of shells. The nourishment sand clearly had high $CaCO_3$ content. Visual inspection of the samples confirmed they were mostly small, broken shell fragments.

The mud content increases from the beach to the offshore area. This is in agreement with sediment maps of Verfaillie, Van Meirvenne, and Van Lancker (2006) and Van Lancker *et al*. (2007), showing a predominance of muddy sediments in the

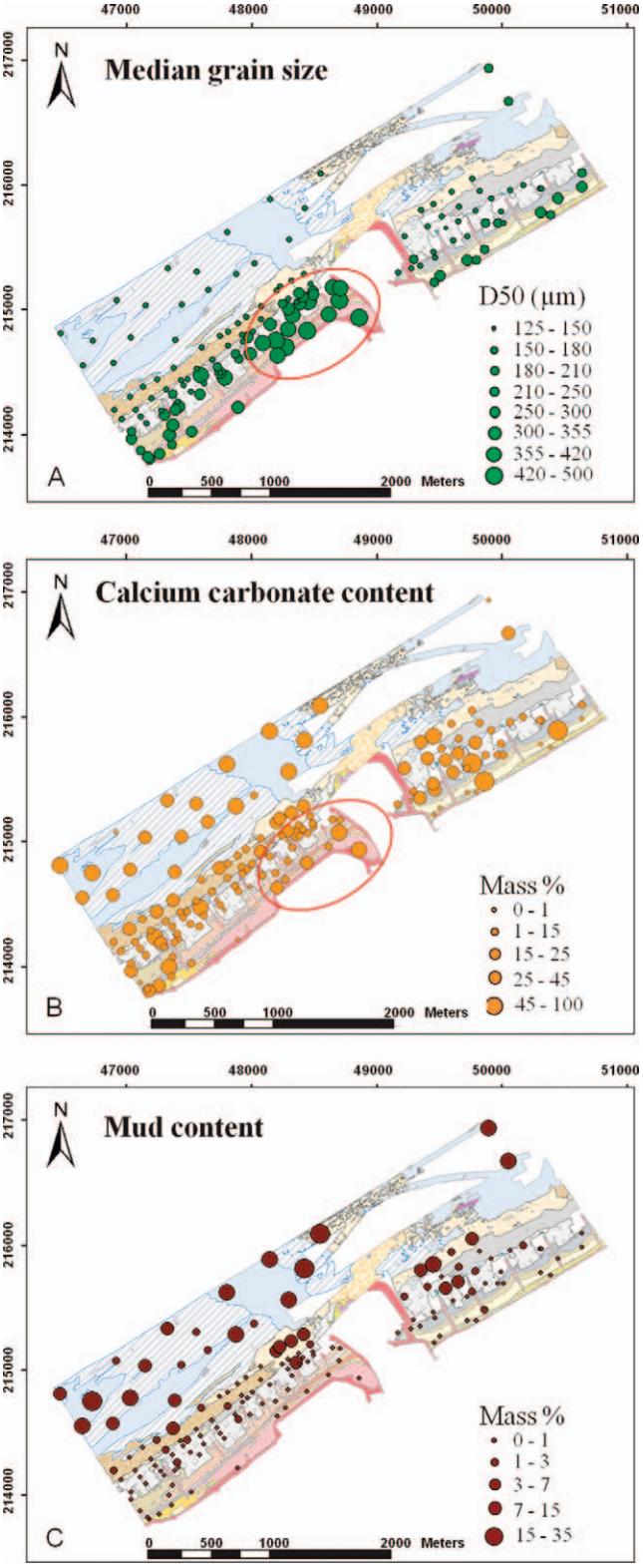


Figure 9. Integrated sedimentary surface facies map overlaid with the sediment sample analyses results: (A) median grain size, (B) calcium carbonate content, and (C) mud content. The red ellipse in the top figures indicates the nourishment area. (Color for this figure is only available in the online version of this paper.)

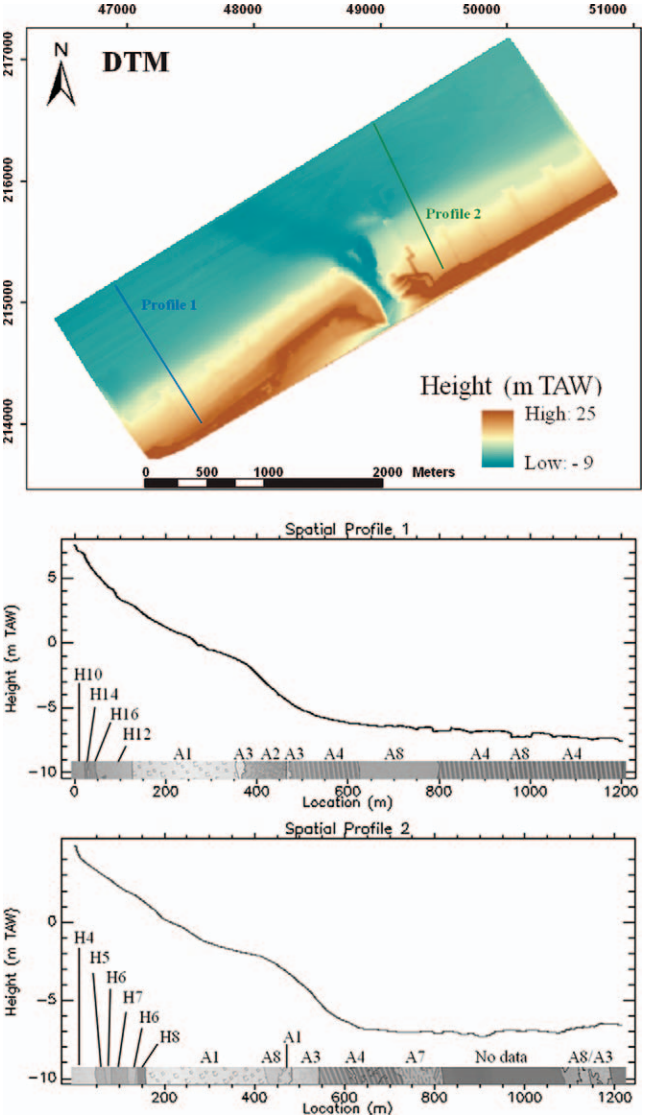


Figure 10. An integrated morphological map could be generated using the LiDAR, echo-sounding, and multibeam data. Cross-profiles, indicating the spatial occurrences of sedimentary surface classes, could be derived by combining the morphological map and the sedimentological classification result. The height is given in meters TAW. (Color for this figure is only available in the online version of this paper.)

coastal zone between Zeebrugge and Ostend. This zone corresponds roughly with the extent of a Holocene mud plate, which also correlates well with the extent of a present-day coastal turbidity maximum (*e.g.,* Fettweis *et al.,* 2009). In the dredged harbor channel, higher percentages of mud prevail, demonstrating that the depth difference of 2 to 3 m enhances mud trapping.

## The Integrated Morphological Map

Using the LiDAR-derived Digital Terrain Model (DTM) and the echo sounder– and multibeam-derived bathymetric data,

an integrated morphological map was generated. The spatial occurrence of sonar sedimentary surface facies classes is clearly related to the bed morphology, bathymetry, and thus benthic activity. The type of sonar class is consequently related to bed dynamics. The two height profiles indicated and plotted in Figure 10 illustrate the depth zonation and the associated classes.

## Morphosedimentary Implications

Comparing the acoustic classes with the sample analysis data indicated a progressively more active seabed toward onshore. The most landward acoustic class, suspension clouds, was located near the low-water mark. It indicates active stirring of the bed during high water under shoaling waves. At the time of the inshore survey, under mild hydrodynamic conditions, this class was found down to –2 m. This depth thus represented the local high-water, fair-weather wave base. At the top and seaward slope of a coast-parallel shoreface bar, homogeneous flat beds were found. They were interpreted as wave-action flat beds.

Class A2, macrobenthos patches, was linked to the steeper parts at the base of the sloping shoreface. The associated shoreface slope ranges from 2 to 5%. The steeper slope is probably the imprint of tidal current flow–related sand movement, while at depths of around 2 to 5 m below MLLWS, the shoreface must also be subject to sediment stirring under higher wave conditions. In this zone, decimeter-scale patches or mounds were identified whose acoustic facies correspond to those described by Degraer *et al*. (2008a) and Van Lancker *et al*. (2012). For both the intertidal and the subtidal areas, these authors evidenced the correspondence of (semi)circular patchy to mottled acoustic facies with dense aggregations of the tube worm *Lanice conchilega*. In Van Lancker *et al*. (2012), fine-scale geomorphological settings were correlated with the presence of macrobenthos, with elongated bands of higher densities of tube-building polychaetes occurring typically along the slopes of sandbanks or the shoreface. In the present study, an elongated band of this type was identified in the lower part of the shoreface, representing the transition between the muddy nearshore and the sandier foreshore. Fine sands with a moderate percentage of silt and clay are the preferred habitat of suspension-feeding polychaetes (Degraer *et al.,* 2008b). These are key species in the *Abra alba* community, which is the richest macrobenthic community in the Belgian part of the North Sea. The limited spatial extension of these bands requires a narrow sampling design when monitoring of macrobenthos is attempted with a view to assessment of ecological status according to European Union directives (*e.g.,* the Water Framework Directive and the Marine Strategy Framework Directive) or impact monitoring of nourishment projects (*e.g.,* Janssen *et al.,* 2008; Speybroeck *et al.,* 2008).

Farther down, the slopes are nearly flat. Marks from beam trawl fisheries were widespread here. The same track imprints were found in sonar and multibeam records that were taken 3 weeks apart. Tracks are generally visible for longer periods in muddy sediments. Both the muddy character and the persistence of the tracks indicate relatively stable beds. In the neighborhood of the trawl marks, wide areas were characterized by "mud with sand patches." The sand patches may represent thin, superficial layers of fresh sediment. This interpretation was corroborated by the class also characterizing the seabed in the dredged navigation channel, where dredging is known to be followed by fresh sedimentation.

Classes with sharp-crested, subaqueous dunes are evidence for mobile beds. The mobile dunes occurred around the harbor dam extension under construction. A few weeks before the inshore surveys, dredged sand had been dumped at the shoreface site of the new eastern harbor dam. Bathymetric monitoring showed that this sand had been redistributed by the currents. The area of occurrence of the dune class clearly maps the extent of this process of sand redistribution.

The 2004 Ostend beach nourishment and the subsequent refills were subject to marked, but local, redistribution of sediments. The nourishment fill undergoes erosion at the high-water mark. The hyperspectral class for white supplied backshore slope sand can be considered evidence for swash erosion (Figure 6). The orange to pink sea-borrowed nourishment sand was characterized by coarse, iron-coated quartz grains and a high proportion of shell fragments. This sand is sorted by wave action: large grains and shell debris are washed out, leaving paler, well-compacted sand as the typical "white" band. Clearly, nourishment sand spread beyond the nourishment area, but the distance was limited to a few hundred meters (compare the "nourishment" classes in Figure 6 with the nourishment areas in Figure 1). Two partial processes can be distinguished. On the one hand, a parallel spread along the coast around the high-water mark is the morphological expression of quite a lot of sediment being pushed both west and east of the nourishment area. This process progresses gradually over time. On the other hand, the intertidal beach below and near the nourishment area received fill sand—but this occurred in a thin layer, pointing to the predominantly bypass role of the intertidal beach. One destination area was seen to be the upper shoreface in front of the nourished beach. Morphological monitoring revealed gradual shallowing. The bed sediment was coarser here than elsewhere on the shoreface, demonstrating the local, coarse nature of the provenance area.

No subaqueous acoustic class could unequivocally be linked to originally nourished sand. Part of the 2004 nourishment was subaquatic (Figure 1 inset): no backtrace in the acoustic sedimentary surface classes was found. Therefore, a transfer of fill sand *via* the shoreface to the offshore or into the harbor channel could not be demonstrated, although it is presumed to take place.

The acoustic classes present offshore prove that the seabed is swept by currents that aim at maintaining the existing equilibrium morphology. A clear illustration of this natural process is the eastern harbor dam construction area, where, in a matter of weeks, dumped sand was lowered by more than 0.5 m and is being actively distributed by dune motion over several hectares downstream (with respect to the dominant flood current). Morphological monitoring showed this area to be erosive. The active dunes are thus the conveyor belt of sand leaving the area. The dredged harbor access channel is a likely local sink, because it has to be kept at a depth of 1 to 2 m below the surrounding seabed by dredging. Morphological monitoring revealed ongoing sedimentation between the dredging works.

The acoustic class found in the harbor access channel is representative of mud, covered with (thin) sand patches. It was interpreted as fresh sedimentation. Shortly after the inshore surveys, works started for the construction of the new western harbor dam. These works will block eastward drift transport and much of the tidal current transport. It is thus expected that accretion will occur to the west of the new harbor dam. The nourishment sand does not make it across the harbor channel. Not one pixel of "nourishment" classes was found on the beaches east of the harbor.

## CONCLUSION

A combination of techniques to study the sedimentological and morphological composition of the back-, fore-, and nearshore continuum, called inshore, is presented here. The study area was the harbor of Ostend, with a history of beach and shoreface nourishment, currently in combination with redesign of the harbor jetties. Optimization of these management actions requires knowledge of sediment dynamics and morphodynamics over the inshore continuum, acquired using the most appropriate monitoring tools.

Quasi-simultaneous airborne hyperspectral and LiDAR campaigns and seaborne acoustic campaigns were conducted to acquire data along the inshore continuum. Both types of campaigns were accompanied by the collection of reference data on the ground. Historical and recent LiDAR data combined with echo-sounding data were used to document the local morphology and to reconstruct the morphological evolution.

The spatial resolution and degree of spatial differentiation of both the airborne hyperspectral and the seaborne sonar images is comparable. This allowed continuous and homogeneous covering of the complete inshore zone, for which a continuous map was created. However, the 60-m-wide overlap area between the hyperspectral and the sonar data sets did not reveal the same appearance of the sediment surface. During high tide, the bed sediment in shallow water was stirred into diffuse suspension clouds by wave action and possibly by the boat's propeller. The suspension clouds prevented the sonar signal from detecting the bed underneath. The suspended bed particles may thus have altered the very appearance of the bed surface. As shown by the hyperspectral data and ground data collected during low tide, the bed sediment at the low-water mark contained very fine sand with a relatively high mud fraction. During high tide, the mud and fine-sand particles were brought into suspension by wave action. As a result, the static muddy sand class, identified during low tide, changed into a dynamic, suspended type of sediment that is not comparable with the static muddy sand; thus, no perfectly corresponding classes could be established in the overlap area.

In contrast to the hyperspectral data, the sonar data did not enable us to derive an acoustic class that was representative of nourishment-related sediment types. Sample data showed coarser, nourishment-derived material on the lower shoreface near the nourishment area. Still, the sonar data did allow the different bed structures to be depicted. These were closely linked with active sediment transport, and the type of sediment structure, together with the spatial occurrence of the structure classes, was successfully linked to morphodynamics.

From an operational point of view, routine monitoring of large coastal stretches using the approach presented here is not feasible. This is due to the narrow hydrometeorological constraints that are required for seaborne and airborne surveys and the expertise and work needed to provide useful and sufficient ground reference data. However, valuable scientific and useful morphodynamic insights were obtained from this study. Consequently, the operational use of complementary seaborne sonar and airborne hyperspectral recordings is recommended, but only for relatively small, specific areas, where considerable benefit is expected from the inshore approach. These areas include economically strategic areas (*e.g.,* harbors) and ecologically dynamic areas (*e.g.,* natural habitat areas).

## ACKNOWLEDGMENTS

The authors thank the Belgian Science Policy Office for providing funding under STEREO project SR/00/125. This study was partially sponsored by the Flemish government, Agency of Maritime Services and Coast, Coastal Division. We also thank the Coastal Division for providing us with the LiDAR data of 2009 and the single-beam data of 2009. We specially thank Stefaan Gysens for his cooperation and providing us with the required information. The authors also thank the members of the inshore steering committee for their critical yet motivating remarks and comments, *viz*. Jacques Populus (Ifremer), Marieke Eleveld (Institute for Environmental Studies, Free University of Amsterdam), Christophe Brière (Deltares), Steven Degraer (Management Unit of the North Sea Mathematical Models), and Koen Trouw (Fides Engineering). Jean-Marie Augustin (Ifremer) is acknowledged for providing assistance during the processing of the acoustic data in SonarScope.

## LITERATURE CITED

Dean, R.G. and Dalrymple, R.A., 2004. *Coastal Processes with Engineering Applications*. Cambridge, UK: Cambridge University Press, 475p.

Degraer, S.; Moerkerke, G.; Rabaut, M.; Van Hoey, G.; Du Four, I.; Vincx, M.; Henriet, J.P., and Van Lancker, V., 2008a. Very-high resolution side-scan sonar mapping of biogenic reefs of the tube-worm *Lanice conchilega*. *Remote Sensing of Environment,* 112, 3323–3328.

Degraer, S.; Verfaillie, E.; Willems, W.; Adriaens, E.; Vincx, M., and Van Lancker, V., 2008b. Habitat suitability modelling as a mapping tool for macrobenthic communities: an example from the Belgian part of the North Sea. *Continental Shelf Research,* 28(3), 369–379.

De Moor, G., 2006. *The Flemish Shore: Geomorphology and Dynamics*. Ostend, Belgium: VLIZ Oostende, 154p [in Flemish].

Deronde, B.; Houthuys, R.; Debruyn, W.; Fransaer, D.; Van Lancker, V., and Henriet, J.P., 2006. Use of airborne hyperspectral data and laserscan data to study beach morphodynamics along the Belgian coast. *Journal of Coastal Research,* 22(5), 1108–1117.

Deronde, B.; Houthuys, R.; Henriet, J.-P.; and Van Lancker, V., 2008a. Monitoring of the sediment dynamics along a sandy shoreline by means of airborne hyperspectral remote sensing and LIDAR: a case study in Belgium. *Earth Surface Processes and Landforms,* 33, 280–294.

Deronde, B.; Kempeneers, P.; Houthuys, R.; Henriet, J.-P., and Van Lancker, V., 2008b. Sedimentfacies classification of a sandy shoreline by means of airborne imaging spectroscopy. *International Journal of Remote Sensing,* 29(15), 4463–4477.

De Wolf, P.; Verwaest, T.; Gysens, S.; Trouw, K.; Martens, C., and De Rouck, J., 2006. Beach nourishment at Ostend, Belgium: design and monitoring. *In: Coastal Engineering 2006: Proceedings of the 30th International Conference* (San Diego, California), Volume 4, pp. 4179–4191.

Fettweis, M.; Houziaux, J.-S.; Du Four, I.; Van Lancker, V.; Baeteman, C.; Mathys, M.; Van den Eynde, D.; Francken, F., and Wartel, S., 2009. Long-term influence of maritime access works on the distribution of cohesive sediments: analysis of historical and recent data from the Belgian nearshore area (southern North Sea). *Geo-Marine Letters,* 29, 321–330.

Janssen, G.; Kleef, H.; Mulder, S., and Tydeman, P., 2008. Pilot assessment of depth related distribution of macrofauna in surf zone along Dutch coast and its implications for coastal management. *Marine Ecology,* 29(Suppl. 1), 186–194.

Kempeneers, P.; De Backer, S.; Deronde, B.; Bertels, L.; Debruyn, W., and Scheunders, P., 2004. Classifying hyperspectral airborne imagery for vegetation survey along coastlines. *In: Proceedings of Geoscience and Remote Sensing Symposium,* (Anchorage, Alaska), Volume 2, pp. 1475–1478.

Leatherman, S.P.; Zhang, K., and Douglas, B.C., 2000. Sea level rise shown to drive coastal erosion. *EOS, Transactions, American Geophysical Union,* 81(6), 55–57.

Maspataud, A.; Ruz, M.-H., and Héquette, A., 2009. Spatial variability in post-storm beach recovery along a macrotidal barred beach, southern North Sea. *In:* Pereira da Silva, C. (ed.) *10th International Coastal Symposium* (Lisbon, Portugal), Journal of Coastal Research, Special Issue No. 56, pp. 88–92.

Mertens, T.; De Wolf, P.; Verwaest, T.; Trouw, K.; De Nocker, L., and Couderé, K., 2008. An integrated master plan for Flanders future coastal safety. *In:* McKee Smith, J. (ed.), *Proceedings of the 31st International Conference on Coastal Engineering* (Hamburg, Germany), pp. 4017–4028.

Mertens, T.; Verwaest, T.; Delgado, R.; Trouw, K., and De Nocker, L., 2011. Book of Abstracts. *In: 32nd International Conference on Coastal Engineering (ICCE 2010)* (Shanghai, China), pp. 1–2.

Smith, D.E.; Raper, S.B.; Zerbini, S., and Sánchez-Arcilla, A., (eds.), 2000. *Sea Level Change and Coastal Processes: Implications for Europe*. Luxembourg: Office for Official Publications of the European Communities, 247p.

Speybroeck, J.; Bonte, D.; Courtens, W.; Gheskiere, T.; Grootaert, P.; Maelfait, J.P.; Provoost, S.; Sabbe, K.; Stienen, E.; Van Lancker, V.; Van Landuyt, W.; Vincx, M., and Degraer, S., 2008. The Belgian sandy beach ecosystem: a review. *Marine Ecology: An Evolutionary Perspective*. 29(Suppl. 1), 171–185.

Stone, G.W. and Orford, J.D., 2004. Storms and their significance in coastal morpho-sedimentary dynamics. *Marine Geology,* 210(1–4), 1–5.

Van Lancker, V.; Du Four, I.; Verfaillie, E.; Deleu, S.; Schelfaut, K.; Fettweis, M.; Van den Eynde, D.; Francken, F.; Monbaliu, J.; Giardino, A.; Portilla, J.; Lanckneus, J.; Moerkerke, G., and Degraer, S., 2007. Management, Research and Budgeting of Aggregates in Shelf Seas Related to Endusers (Marebasse). Belgian Science Policy, EV/18. http://www.belspo.be/belspo/organisation/publ/pub_ostc/EV/rEV18_en.pdf (accessed March 10, 2012).

Van Lancker, V.; Moerkerke, G.; Du Four, I.; Verfaillie, E.; Rabaut, M., and Degraer, S., 2012. Fine-scale geomorphological mapping for the prediction of macrobenthic occurrences in shallow marine environments, Belgian part of the North Sea. *In:* Harris, P. and Baker, E.K. (eds.), *Seafloor Geomorphology as Benthic Habitat: GeoHab Atlas of Seafloor Geomorphic Features and Benthic Habitats*. London: Elsevier Insights, pp. 251–260.

Verfaillie, E.; Van Meirvenne, M., and Van Lancker, V., 2006. Multivariate geostatistics for the predictive modelling of the surficial sand distribution in shelf seas. *Continental Shelf Research,* 26(19), 2454–2468.